© 2002 The Chemical Society of Japan Bull. Chem. Soc. Jpn., 75, 99–107 (2002)

Heterodinuclear $M^{II}Ni^{II}$ (M = Co, Ni, Cu, Zn) Complexes of a Macrocyclic Compartmental Ligand. Anomalous EPR of $Cu^{II}Ni^{II}$ Complex by Coordination of 1-Methylimidazole

Ko-ji Inoue, Masaaki Ohba, and Hisashi Ōkawa*

Department of Chemistry, Faculty of Science, Kyushu University, Hakozaki, Higashiku 6-10-1, Fukuoka 812-8581

(Received August 3, 2001)

A phenol-based macrocyclic compartmental ligand, $(L^{2;2})^{2-}$, having $N(amine)_2O_2$ and $N(imine)_2O_2$ metal binding sites sharing two phenolic oxygen atoms, has formed the following heterodinuclear $M^{II}Ni^{II}$ complexes: $[CoNi(L^{2;2})(AcO)]PF_6 \cdot CH_3CN$ (**1**), $[NiNi(L^{2;2})(AcO)]PF_6$ (**2**), $[CuNi(L^{2;2})(AcO)]PF_6$ (**3**) and $[ZnNi(L^{2;2})(AcO)]PF_6 \cdot CH_3CN$ (**4**). Furthermore, $[CuNi(L^{2;2})(CH_3CN)](PF_6)_2 \cdot CH_3CN$ (**3′**) was obtained when **3** was recrystallized from acetonitrile. X-ray crystallographic studies for **1, 2, 3′** and **4** demonstrate that the M^{II} resides in the $N(amine)_2O_2$ site and the Ni^{II} in the $N(imine)_2O_2$ site. The Ni^{II} in the $N(imine)_2O_2$ site has a planar geometry and is diamagnetic in all the complexes. The Co^{II} of **1** and the Ni^{II} of **2** in the $N(amine)_2O_2$ site have a six-coordinate geometry together with a bidentate acetate group. The Cu^{II} in **3′** has a five-coordinate geometry together with one acetonitrile molecule, and the Zn^{II} in **4** has a square-pyramidal geometry together with a unidentate acetate group. Complex **3′** in DMF combines 1-methylimidazole (MeIm) at the axial site of the Ni^{II} and the MeIm adduct in frozen DMF solution at 77.4 K shows EPR signals of $g_{\parallel} = 2.06$ and $g_{\perp} = 2.26$ with a multi-line structure superimposed on the $g_{\parallel}$ component ($A_{\parallel} = 15.8 \times 10^{-4}$ cm^{-1}). The EPR signals are ascribed to the spin-doublet ground state ($S_T = 1/2$) of antiferromagnetically coupled $Cu^{II}(S = 1/2) - Ni^{II}(S = 1)$, and the multi-line structure is explained by considering hyperfine interaction with Cu nucleus ($A_{Cu} = 50.0 \times 10^{-4}$ cm^{-1}) and superhyperfine interaction with N nucleus of MeIm ($A_N = 15.0 \times 10^{-4}$ cm^{-1}).

Macrocyclic compartmental ligands whose two metal-binding sites are not equivalent with respect to the cavity size, coordination number, geometric requirement, or the nature of donor atoms are important for studies of heterodinuclear metal complexes.[1] Phenol-based macrocyclic ligands of the type in Chart 1 (abbreviated as $(L^{m;n})^{2-}$), having two dissimilar $N(amine)_2O_2$ and $N(imine)_2O_2$ metal-binding sites (aminic and iminic sites, respectively) sharing the phenolic oxygen atoms, have been developed for our purpose to study heterodinuclear metal complexes.[2–5] The macrocyclic ligands have been synthesized by a template reaction as mononuclear $[Cu(L^{m;n})]$ and dinuclear $[PbCu(L^{m;n})](ClO_4)_2$, both of which can be used as precursors for transition metal heterodinuclear complexes. Mononuclear $[Cu(L^{m;n})]$ complexes have the Cu^{II} in the iminic site and accommodate a second M^{II} ion in the aminic site to afford $M^{II}Cu^{II}$ complexes $[MCu(L^{m;n})Cl_2]^{2c-2e}$ ("M_aM_b" complex and the $[M_aM_b(L^{m;n})]^{2+}$ formulation mean that the M_a resides in the aminic site and the M_b resides in the iminic site). The reaction of $[PbCu(L^{m;n})](ClO_4)_2$ with M^{II} sulfate caused the migration of the Cu^{II} from the iminic site to the aminic site to afford $Cu^{II}M^{II}$ complexes.[2b,2d,2e] Thus, the macrocyclic ligands show site specificity of metal ions providing $Cu^{II}M^{II}$ or $M^{II}Cu^{II}$ complexes, depending upon the synthetic method or the nature of the counter ion used.

We are interested in studying physicochemical properties and functions of heterodinuclear complexes in view of interaction or interplay of dissimilar metal ions in close proximity. In this work, the following $M^{II}Ni^{II}$ complexes have been derived from $(L^{2;2})^{2-}$: $[CoNi(L^{2;2})(AcO)]PF_6 \cdot CH_3CN$ (**1**), $[NiNi(L^{2;2})(AcO)]PF_6$ (**2**), $[CuNi(L^{2;2})(AcO)]PF_6$ (**3**) and $[ZnNi(L^{2;2})AcO)]PF_6 \cdot CH_3CN$ (**4**). Furthermore, $[CuNi(L^{2;2})(CH_3CN)](PF_6)_2 \cdot CH_3CN$ (**3′**) was obtained when **3** was recrystallized from acetonitrile. They are structurally characterized and their physicochemical properties have been studied. Our focus is placed on complex **3′** that combines 1-methylimidazole (MeIm) at the axial site of the Ni^{II} and exhibits anomalous EPR of $g_{\parallel} = 2.06$ and $g_{\perp} = 2.26$ with a multi-line structure superimposed on the $g_{\parallel}$ component ($A_{\parallel} = 15.8 \times 10^{-4}$ cm^{-1}).

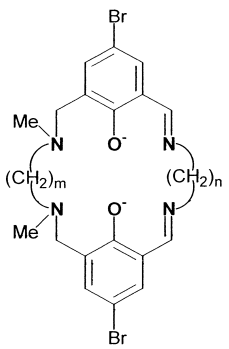

Chart 1. Chemical structure of $(L^{m;n})^{2-}$.

Experimental

Physical Measurements. Elemental analyses of C, H, and N were obtained at The Service Center of Elemental Analysis of

Kyushu University. Metal analyses were made on a Shimadzu AA-680 Atomic Absorption/Flame Emission Spectrophotometer. Infrared spectra were recorded on a Perkin Elmer BX FT-IR system using KBr disks. Fast atom bombardment (FAB) mass spectra were recorded on a JMS-SX/SX102A Tundem mass spectrometer using *m*-nitrobenzylalcohol as the matrix. Electronic absorption spectra were recorded on a Shimadzu UV-3100PC spectrophotometer. Magnetic susceptibilities of powdered samples were measured on a Quantum Design MPMS XL SQUID susceptometer in the temperature range of 2–300 K. Diamagnetic corrections for the constituting atoms were carried out using Pascal's constants.[6] X-band EPR spectra were measured on a JEOL JEX-FE3X spectrometer in frozen DMF solution at liquid nitrogen temperature. Cyclic voltammograms were measured using a BAS CV-50W electrochemical analyzer in acetonitrile solution containing tetra(*n*-butyl)ammonium perchlorate (TBAP) as the supporting electrolyte (**Caution!** TBAP is explosive and should be handled with great care). A three-electrode cell was used which was equipped with a glassy carbon working electrode, a platinum coil as the counter electrode and a Ag/Ag^+ (TBAP/acetonitrile) electrode as the reference.

Preparation. Unless otherwise stated, chemical reagents were purchased from commercial sources and used without further purification. The synthesis of *N*,*N*′-dimethyl-*N*,*N*′-ethylenedi(5-bromo-3-formyl-2-hydroxybenzylamine) (H_2L') was described in our previous paper.[2a]

[Ni($L^{2;2}$)]. A mixture of H_2L' (5.00 g, 9.72 mmol) and nickel(II) acetate tetrahydrate (2.42 g, 9.72 mmol) in methanol (100 cm^3) was refluxed for three hours. To the resulting pale green solution was dropwise added a solution of ethylenediamine (0.58 g, 9.72 mmol) in methanol (10 cm^3), and the mixture was refluxed for one hour to give an orange microcrystalline powder. It was collected by suction filtration, thoroughly washed with methanol and dried in vacuo. The yield was 5.0 g (86%). Calcd. for $C_{22}H_{24}Br_2N_4NiO_2$: C, 44.40; H, 4.06; N, 9.41; Ni, 9.86%. Found: C, 44.23; H, 3.98; N, 9.38; Ni, 10.24%. Selected IR [ν / cm^{-1}] using KBr: 1618, 1536, 1445, 1220.

[Ni($HL^{2;2}$)]PF_6·0.5H_2O. To a suspension of [Ni($L^{2;2}$)] (5.0 g, 8.4 mmol) in methanol (100 cm^3) was added excess KPF_6 (4.6 g, 25 mmol), and the mixture was stirred at the reflux temperature overnight. Unreacted [Ni($L^{2;2}$)] was removed by filtration, and the filtrate was diffused with ether to give red crystals. They were separated, washed with methanol and dried in vacuo. The yield was 5.6 g (90%). Calcd for $C_{22}H_{26}Br_2F_6N_4NiO_{2.5}P$: C, 35.22; H, 3.49; N, 7.47; Ni, 7.82%. Found: C, 35.22; H, 3.59; N, 7.29; Ni, 7.57%. Selected IR [ν/cm^{-1}] using KBr: 1613, 1450, 839, 557. UV–vis [λ/nm (ε/M^{-1} cm^{-1})] in DMF: 418 (8670), 520 (269).

[PbNi($L^{2;2}$)($AcO)_2$]. A methanol solution (50 cm^3) of lead(II) acetate trihydrate (320 mg, 0.84 mmol) was added to a hot suspension of [Ni($L^{2;2}$)] (500 mg, 0.84 mmol) in methanol (50 cm^3), and the mixture was stirred at the reflux temperature for five hours. The resulting red solution was evaporated to dryness, the residue was dissolved in DMF and the DMF solution was diffused with 2-propanol to form red crystals. The yield was 495 mg (65%). Calcd for $C_{26}H_{30}Br_2N_4NiO_6Pb$: C, 33.93; H, 3.29; N, 6.09; Ni, 6.38%. Found: C, 34.24; H, 3.58; N, 6.23; Ni, 6.82%. Selected IR [ν/cm^{-1}]: 1614, 1572, 1448, 1398, 1331. UV–vis [λ/nm (ε / M^{-1} cm^{-1})] in DMF: 413 (7990), 520 (288).

[CoNi($L^{2;2}$)(AcO)]PF_6·CH_3CN (1). A solution of [PbNi($L^{2;2}$)($AcO)_2$] (500 mg, 0.54 mmol), cobalt(II) sulfate heptahydrate (150 mg, 0.54 mmol) and potassium hexafluorophosphate (150 mg, 1.09 mmol) in methanol (50 cm^3) was refluxed for one hour. The resulting $PbSO_4$ was separated by filtration and the filtrate was evaporated to dryness. The residue was extracted with acetonitrile (10 cm^3) and the extract was diffused with ether to form reddish brown crystals. The yield was 230 mg (48%). Calcd for $C_{26}H_{30}Br_2CoF_6N_5NiO_4P$: C, 34.73; H, 3.36; N, 7.79; Co, 6.55; Ni, 6.53%. Found: C, 34.34; H, 3.32; N, 7.73; Co, 6.87; Ni, 6.84%. Selected IR [ν/cm^{-1}]: 2258, 1621, 1540, 1450, 1298, 842. UV–vis [λ/nm (ε / M^{-1} cm^{-1})] in DMF: 386 (5800), 520 (147), 1240(8).

[NiNi($L^{2;2}$)(AcO)]PF_6 (2). This was obtained as reddish brown crystals in a way similar to that for **1**, using nickel(II) sulfate hexahydrate (140 mg, 0.54 mmol) instead of $CoSO_4$·$7H_2O$. The yield was 370 mg (80%). Calcd for $C_{24}H_{27}Br_2F_6N_4Ni_2O_4P$: C, 33.59; H, 3.17; N, 6.53; Ni, 13.68%. Found: C, 33.83; H, 3.19; N, 6.61; Ni, 14.03%. Selected IR [ν/cm^{-1}]: 1631, 1538, 1450, 1287, 841. UV–vis [λ/nm (ε / M^{-1} cm^{-1})] in CH_3CN: 383 (5890), 520 (144), 652 (18), 1030 (11).

[CuNi($L^{2;2}$)(AcO)]PF_6 (3). This was obtained as reddish brown crystals in a way similar to that for **1** except for the use of copper(II) sulfate pentahydrate (140 mg, 0.54 mmol) instead of $CoSO_4$·$7H_2O$. The yield was 270 mg (58%). Calcd for $C_{24}H_{27}Br_2CuF_6N_4NiO_4P$: C, 33.41; H, 3.15; N, 6.49; Cu, 7.37; Ni, 6.80%. Found: C, 33.75; H, 3.63; N, 6.56; Cu, 7.22; Ni, 7.32%. Selected IR [ν/cm^{-1}]: 1628, 1567, 1450, 1300, 840. UV–vis [λ/nm (ε / M^{-1} cm^{-1}) in DMF: 390 (6480), 520 (310), 670 (86).

A portion of **3** was dissolved in acetonitrile and the solution was diffused with ether to give [CuNi($L^{2;2}$)(CH_3CN)]($PF_6)_2$·CH_3CN (**3′**) as reddish brown crystals. Calcd. for $C_{26}H_{30}Br_2CuF_{12}N_6NiO_2P_2$: C, 30.30; H, 2.93; N, 8.15; Cu, 6.16; Ni, 5.69%. Found: C, 30.17; H, 2.86; N, 7.99; Cu, 6.53; Ni, 5.35%.

[ZnNi($L^{2;2}$)(AcO)]PF_6·CH_3CN (4). This was obtained as red crystals in a way similar to that for **1** using zinc(II) sulfate heptahydrate (160 mg, 0.54 mmol). The yield was 360 mg (74%). Calcd for $C_{26}H_{30}Br_2F_6N_5NiO_4PZn$: C, 34.48; H, 3.34; N, 7.73; Ni, 6.84; Zn, 7.22%. Found: C, 34.43; H, 3.40; N, 7.84; Ni, 6.85; Zn, 7.63%. Selected IR [ν/cm^{-1}]: 2258, 1621, 1557, 1450, 1300, 842. UV–vis [λ/nm (ε / M^{-1} cm^{-1})] in DMF: 387 (4750), 520 (150).

X-ray Crystallography. Each single crystal of [Ni($HL^{2;2}$)]PF_6·0.5H_2O, [PbNi($L^{2;2}$)($AcO)_2$], [CoNi($L^{2;2}$)(AcO)]PF_6·CH_3CN (**1**), [NiNi($L^{2;2}$)(AcO)]PF_6 (**2**), [CuNi($L^{2;2}$)(CH_3CN)]($PF_6)_2$·CH_3CN (**3′**) and [ZnNi($L^{2;2}$)(AcO)]PF_6·CH_3CN (**4**) was mounted on a glass fiber and coated with epoxy resin. Crystallographic measurements were carried out on a Rigaku AFC7R diffractometer with graphite monochromated Mo-$K\alpha$ radiation (λ = 0.71069 Å) and a 12 kW rotating anode generator. Cell constants and the orientation matrix for the data collection were obtained from 25 reflections and the ω–2θ scan mode was used for the intensity collections at 293 ± 1 K. Pertinent crystallographic parameters are summarized in Table 1.

Three standard reflections were monitored every 150 measurements. A linear correction factor was applied to the data to account for the decay phenomena observed. Intensity data were corrected for Lorentz and polarization effects. The structures were solved by the direct method and expanded using the Fourier techniques. The non-hydrogen atoms were refined anisotropically. Hydrogen atoms were included in the structure analysis but not refined. Computations were carried out on an IRIS O_2 computer using TEXSAN crystallographic software package.[7]

Crystallographic data have been deposited at the CCDC, 12 Union Road, Cambridge CB2 1EZ, UK and copies can be obtained on request, free of charge, by quoting the publication citation and deposition number CCDC 172355–172340. The data are

Table 1. Crystallographic Parameters for $[Ni(HL^{2;2})]PF_6 \cdot 0.5H_2O$, $[PbNi(AcO)_2(L^{2;2})]$, $[CoNi(L^{2;2})(AcO)]PF_6 \cdot CH_3CN$ (**1**), $[NiNi(L^{2;2})(AcO)]PF_6$ (**2**), $[CuNi(L^{2;2})(CH_3CN)](PF_6)_2 \cdot CH_3CN$ (**3′**) and $[ZnNi(L^{2;2})(AcO)]PF_6 \cdot CH_3CN$ (**4**)

Complex	$[Ni(HL^{2;2})]PF_6 \cdot 0.5H_2O$	$[PbNi(L^{2;2})(AcO)_2]$	**1**	**2**	**3′**	**4**
Formula	$C_{22}H_{26}N_4Br_2F_6NiO_{2.5}P$	$C_{26}H_{30}N_4Br_2NiO_6Pb$	$C_{26}H_{30}N_5Br_2CoF_6NiO_4P$	$C_{24}H_{27}N_4Br_2F_6Ni_2O_4P$	$C_{24}H_{27}N_4Br_2CuF_6NiO_4P$	$C_{26}H_{30}N_5Br_2F_6NiO_4PZn$
F. w.	748.94	920.25	898.96	857.67	1030.54	905.41
Crystal color	red	red	reddish brown	reddish brown	reddish brown	red
Crystal size/mm^3	0.20×0.20×0.20	0.30×0.20×0.18	0.20×0.10×0.20	0.20×0.20×0.20	0.20×0.14×0.08	0.20×0.20×0.20
Crystal system	triclinic	monoclinic	triclinic	monoclinic	triclinic	triclinic
Space group	$P\bar{1}$(#2)	$P2_1/c$(#14)	$P\bar{1}$(#2)	$P2_1/c$(#14)	$P\bar{1}$(#2)	$P\bar{1}$(#2)
a/Å	10.968(8)	11.709(4)	14.250(2)	8.388(2)	11.351(8)	14.216(3)
b/Å	13.13(1)	8.795(2)	15.428(2)	14.304(2)	17.14(1)	15.561(3)
c/Å	10.89(1)	28.96(1)	8.1355(9)	24.655(3)	9.833(9)	8.145(3)
α/°	109.82(6)		104.10(1)		98.75(6)	103.31(2)
β/°	99.97(8)	97.41(3)	91.71(1)	91.73(2)	92.49(3)	92.49(3)
γ/°	71.23(6)		111.119(9)		107.24(6)	111.88(2)
V/Å^3	1392(2)	2957(1)	1604.4(4)	2956.8(8)	1804(2)	1610.4(8)
Z	2	4	2	4	2	2
D_{calcd}/g cm^{-3}	1.786	2.067	1.861	1.927	1.897	1.867
μ(Mo-$K\alpha$)/ cm^{-1}	37.02	90.88	37.28	41.15	35.19	39.44
No. of reflections	4226	4320	3009	3914	4812	3871
	($I > 3.00\sigma(I)$)	($I > 3.00\sigma(I)$)	($I > 2.00\sigma(I)$)	($I > 3.00\sigma(I)$)	($I > 3.00\sigma(I)$)	($I > 3.00\sigma(I)$)
F(000)	746.00	1768.00	894.00	1704.00	1018.00	900.00
R	0.047	0.052	0.057	0.040	0.037	0.046
R_w	0.069	0.084	0.066	0.057	0.050	0.067

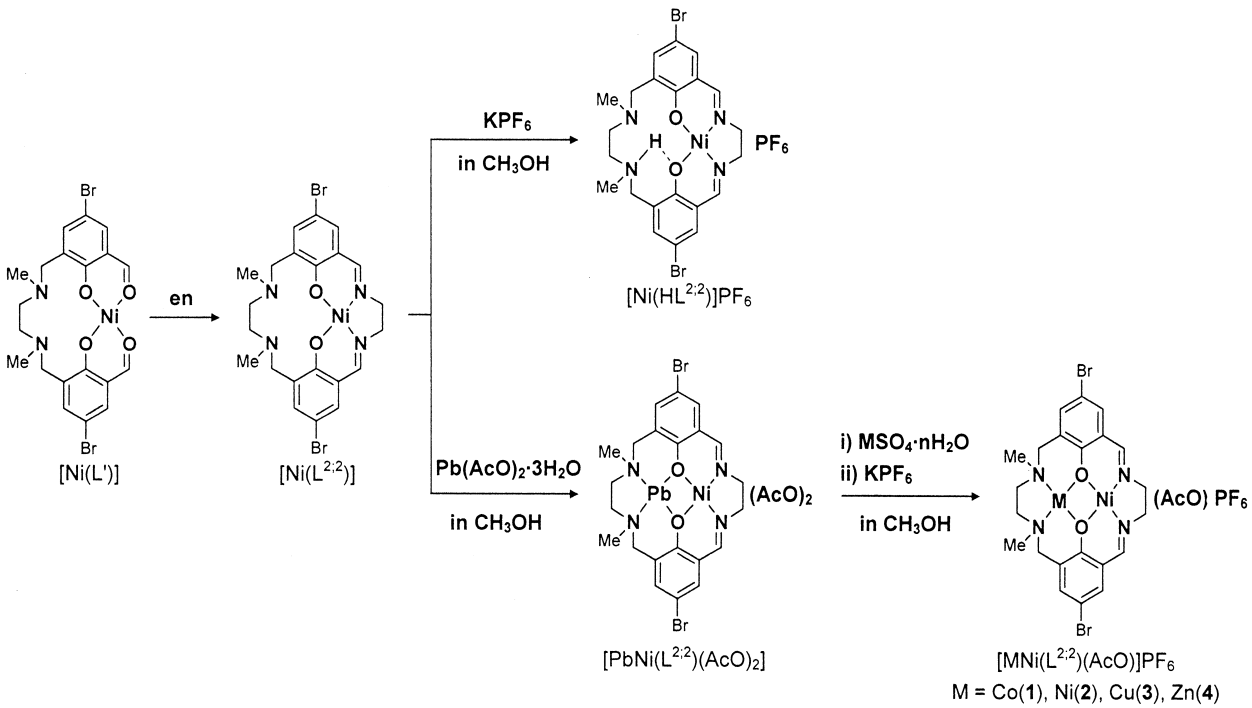

Scheme 1. Synthetic scheme of complexes.

also deposited as Document No. 75005 at the Office of the Editor of Bull. Chem. Soc. Jpn.

Results and Discussion

Preparation and Characterization by FAB Mass Spectrometry. The synthetic method of the $M^{II}Ni^{II}$ complexes (**1**–**4**) is schematically shown in Scheme 1. The mononuclear Ni^{II} complex $[Ni(L^{2;2})]$ was obtained in a good yield by the reaction of $[Ni(L')]$ with ethylenediamine in methanol. $[Ni(L^{2;2})]$ has the Ni^{II} in the iminic site judged from the d–d band maximum at 520 nm[8] and the diamagnetic nature of the complex. This is proved by X-ray crystallographic study for $[Ni(HL^{2;2})]PF_6 \cdot 0.5H_2O$ (to be discussed later), which was unexpectedly obtained when $[Ni(L^{2;2})]$ was treated with KPF_6 in methanol. $[Ni(L^{2;2})]$, however, proved not to be a good precursor for heterodinuclear $M^{II}Ni^{II}$ complexes because of its low

solubility in common solvents. For example, in the reaction of $[Ni(L^{2;2})]$ with M^{II} chloride in methanol, the resulting product, $[MNi(L^{2;2})Cl_2]$, was always contaminated with a large amount of intact $[Ni(L^{2;2})]$. On the other hand, $[PbNi(L^{2;2})(AcO)_2]$ derived from $[Ni(L^{2;2})]$ by the reaction with $Pb(CH_3COO)_2 \cdot 3H_2O$ was found to be considerably soluble in methanol. The transmetallation reaction using M^{II} sulfate salts in the presence of KPF_6 afforded $[MNi(L^{2;2})(AcO)]PF_6$ (**1**–**4**).

FAB mass spectrometric studies for **2** (NiNi) indicated two molecular ion peaks centered around m/z = 652 and 711; these correspond to $\{NiNi(L^{2;2})\}^+$ and $\{NiNi(L^{2;2})(AcO)\}^+$, respectively. Similarly, FAB mass studies for **3** (CuNi) indicated two molecular ion peaks centered around m/z = 657 and 718 that correspond to $\{CuNi(L^{2;2})\}^+$ and $\{CuNi(L^{2;2})(AcO)\}^+$, respectively. Complex **1** (CoNi) showed two molecular ion peaks centered around m/z = 712 and 805 that are ascribed to $\{CoNi(L^{2;2})(AcO)\}^+$ and $\{CoNi(L^{2;2})(mnbo)\}^+$ ($mnbo^-$ = *m*-nitrobenzylalcolate), respectively. Similarly, **4** (ZnNi) showed two molecular ion peaks corresponding to $\{ZnNi(L^{2;2})(AcO)\}^+$ and $\{ZnNi(L^{2;2})(mnbo)\}^+$. The $mnbo^-$ in the $\{MNi(L^{2;2})(mnbo)\}^+$ species recognized for **1** and **4** originates from the matrix used for FAB mass measurements.

Crystal Structures. $[Ni(HL^{2;2})]PF_6 \cdot 0.5H_2O$ and $[PbNi(L^{2;2})(AcO)_2]$. ORTEP[9] views of $[Ni(HL^{2;2})]PF_6 \cdot 0.5H_2O$ and $[PbNi(L^{2;2})(AcO)_2]$ are shown in Figs. 1 and 2, respectively, together with the atom numbering schemes. The relevant bond distances and angles are given in Tables 2 and 3, respectively.

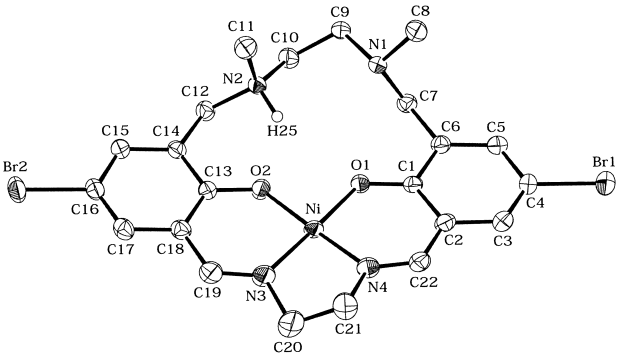

Fig. 1. An ORTEP view of $[Ni(HL^{2;2})]PF_6 \cdot 0.5H_2O$ with the atom numbering scheme.

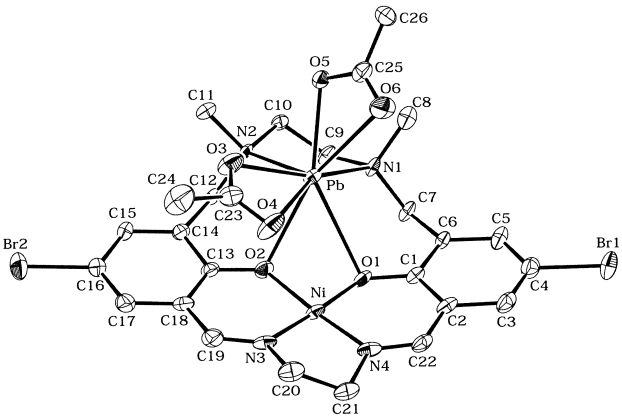

Fig. 2. An ORTEP view of $[PbNi(L^{2;2})(AcO)_2]$ with the atom numbering scheme.

The crystallographic result clearly demonstrates that the Ni^{II} resides in the iminic site and assumes a planar geometry similar to [Ni(salen)].[10] The Ni–N and Ni–O bond distances range from 1.825(3) to 1.847(4) Å. Such short bond distances are characteristic of low-spin Ni^{II}. The proton is bonded to N2 and hydrogen-bonded to O2.

In the crystal of $[PbNi(L^{2;2})(AcO)_2]$, the Ni^{II} resides in the iminic site and assumes a nearly planar geometry with the Ni-to-donor bond distances of 1.817(8)–1.842(9) Å. The Pb^{II} in the aminic site assumes an eight-coordinate geometry together with two bidentate acetate groups. The Pb–N1 and Pb–O1 bond distances (2.967(8) and 3.047(7) Å, respectively) are significantly long relative to the Pb–N2 and Pb–O2 distances (2.588(7) and 2.737(7) Å, respectively). The Pb atom is displaced by 1.892(4) Å from the $N(amine)_2O_2$ least-squares plane toward the acetate groups. The $N(imine)_2O_2$ least-squares plane and the $N(amine)_2O_2$ least-squares plane are bent at the O1–O2 edge with a large dihedral angle of 26.8(2)°.

Table 2. Selected Bond Lengths (Å) and Angles (°) for $[Ni(HL^{2;2})]PF_6.0.5H_2O$

Ni–O(1)	1.825(3)	Ni–N(4)	1.836(4)
Ni–O(2)	1.831(3)	N(2)–H(25)	0.947(3)
Ni–N(3)	1.847(4)	O(2)···H(25)	1.899(3)
O(1)–Ni–O(2)	82.7(1)	O(2)–Ni–N(3)	94.4(2)
O(1)–Ni–N(3)	176.1(2)	O(2)–Ni–N(4)	178.1(2)
O(1)–Ni–N(4)	95.4(2)	N(3)–Ni–N(4)	87.4(2)

Table 3. Selected Bond Lengths (Å) and Angles (°) for $[PbNi(L^{2;2})(AcO)_2]$

Pb–O(1)	3.047(7)	Pb–N(2)	2.588(7)
Pb–O(2)	2.737(7)	Ni–O(1)	1.817(8)
Pb–O(3)	2.351(9)	Ni–O(2)	1.839(7)
Pb–O(4)	2.93(1)	Ni–N(3)	1.842(9)
Pb–O(5)	2.389(7)	Ni–N(4)	1.836(9)
Pb–O(6)	2.779(9)		
Pb–N(1)	2.967(8)	Pb···Ni	3.325(2)
Pb–O(1)–Ni	82.0(2)	O(3)–Pb–N(1)	148.7(3)
Pb–O(2)–Ni	91.0(3)	O(3)–Pb–N(2)	80.0(3)
O(1)–Pb–O(2)	48.7(2)	O(4)–Pb–O(5)	116.7(3)
O(1)–Pb–O(3)	130.8(3)	O(4)–Pb–O(6)	91.4(3)
O(1)–Pb–O(4)	97.8(2)	O(4)–Pb–N(1)	158.8(2)
O(1)–Pb–O(5)	141.7(2)	O(4)–Pb–N(2)	120.7(3)
O(1)–Pb–O(6)	118.0(2)	O(5)–Pb–O(6)	49.5(2)
O(1)–Pb–N(1)	61.2(2)	O(5)–Pb–N(1)	82.7(3)
O(1)–Pb–N(2)	98.0(2)	O(5)–Pb–N(2)	79.0(3)
O(2)–Pb–O(3)	86.0(3)	O(6)–Pb–N(1)	95.8(3)
O(2)–Pb–O(4)	78.5(3)	O(6)–Pb–N(2)	128.2(3)
O(2)–Pb–O(5)	149.7(2)	N(1)–Pb–N(2)	69.1(2)
O(2)–Pb–O(6)	160.8(2)	O(1)–Ni–O(2)	82.1(3)
O(2)–Pb–N(1)	88.5(2)	O(1)–Ni–N(3)	176.9(4)
O(2)–Pb–N(2)	70.8(2)	O(1)–Ni–N(4)	95.4(4)
O(3)–Pb–O(4)	47.8(3)	O(2)–Ni–N(3)	95.0(4)
O(3)–Pb–O(5)	86.7(3)	O(2)–Ni–N(4)	175.6(4)
O(3)–Pb–O(6)	99.5(3)	N(3)–Ni–N(4)	87.5(4)

The asymmetric nitrogen atoms N1 and N2 have *S* and *R* configurations, respectively. The two methyl groups attached to N1 and N2 are situated *cis* with respect to the $N(amine)_2O_2$ least-squares plane.

$[CoNi(L^{2;2})(AcO)]PF_6 \cdot CH_3CN$ (1). An ORTEP drawing of **1** is given in Fig. 3, together with the atom numbering scheme. The selected bond distances and angles are given in Table 4.

The complex has a discrete heterodinuclear core with the Co^{II} in the aminic site and the Ni^{II} in the iminic site. The complex exists in two distinct forms, A and B, with respect to the configuration about N1 (Fig. 4); the configuration about N1 is *S* in form A, but *R* in form B. The probabilities for A and B are 75 and 25%, respectively. The two methyl groups attached to the asymmetric nitrogen atoms N1 and N2 are situated *cis* in form A, but *trans* in form B. Figure **3** shows the crystal structure of form A. The acetate group coordinates to the Co as a chelating bidentate ligand providing a distorted six-coordinate geometry about the metal. The Co-to-donor bond distances range from 2.041(6) to 2.185(7) Å. The Co is 0.837(4) Å displaced from the $N(amine)_2O_2$ least-squares plane toward the acetate ligand. The Ni^{II} in the iminic site has a planar geometry with Ni-to-donor distances of 1.825(8)–1.844(6) Å. The Co–Ni intermetallic separation is 2.991(2) Å. The $N(amine)_2O_2$ least-squares plane and the $N(imine)_2O_2$ least-squares plane are bent at the O1–O2 edge with a dihedral angle of 11.1(2)°.

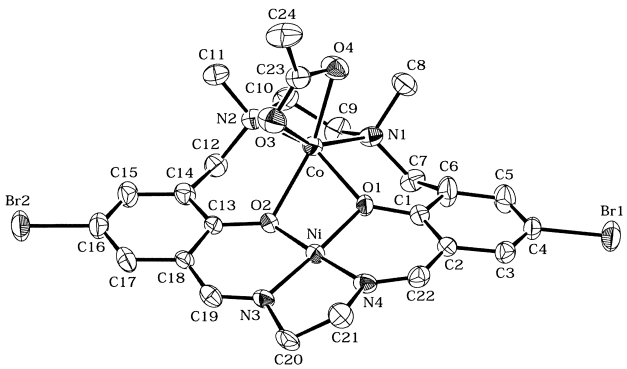

Fig. 3. An ORTEP view of $[CoNi(L^{2;2})(AcO)]PF_6 \cdot CH_3CN$ (**1**) with the atom numbering scheme.

Table 4. Selected Bond Lengths (Å) and Angles (°) for $[CoNi(L^{2;2})(AcO)]PF_6 \cdot CH_3CN$] (**1**)

Co–O(1)	2.041(6)	Ni–O(1)	1.832(6)
Co–O(2)	2.152(6)	Ni–O(2)	1.844(6)
Co–O(3)	2.069(7)	Ni–N(3)	1.825(8)
Co–O(4)	2.184(7)	Ni–N(4)	1.836(8)
Co–N(1)	2.133(8)		
Co–N(2)	2.136(8)	Co···Ni	2.991(2)
Co–O(1)–Ni	101.0(3)	O(3)–Co–N(1)	153.5(3)
Co–O(2)–Ni	96.7(3)	O(3)–Co–N(2)	98.4(3)
O(1)–Co–O(2)	69.9(2)	O(4)–Co–N(1)	93.6(3)
O(1)–Co–O(3)	103.1(3)	O(4)–Co–N(2)	100.9(3)
O(1)–Co–O(4)	108.7(3)	N(1)–Co–N(2)	84.9(3)
O(1)–Co–N(1)	85.5(3)		
O(1)–Co–N(2)	149.4(3)	O(1)–Ni–O(2)	81.6(3)
O(2)–Co–O(3)	88.3(3)	O(1)–Ni–N(3)	176.8(3)
O(2)–Co–O(4)	147.6(3)	O(1)–Ni–N(4)	94.9(3)
O(2)–Co–N(1)	118.1(3)	O(2)–Ni–N(3)	96.6(3)
O(2)–Co–N(2)	89.5(3)	O(2)–Ni–N(4)	176.1(3)
O(3)–Co–O(4)	60.0(3)	N(3)–Ni–N(4)	87.0(4)

$[NiNi(L^{2;2})(AcO)]PF_6$ (2). An ORTEP view of **2** is given in Fig. 5 together with the atom numbering scheme. The relevant bond distances and angles are given in Table 5.

The Ni1 in the aminic site has a six-coordinate geometry together with a bidentate acetate group. The Ni-to-donor bond distances range from 2.076(4) to 2.117(4) Å. The Ni is 0.776(2) Å displaced from the basal $N(amine)_2O_2$ least-squares plane toward the acetate group. The N2 in the iminic site assumes a planar geometry with N2-to-donor distances of 1.820(4)–1.861(4) Å. The asymmetric nitrogen atoms N1 and N2 have the same *S* configuration. The two methyl groups attached to N1 and N2 are situated *trans* with respect to the mean molecular plane. The $N(amine)_2O_2$ least-squares plane and the $N(imine)_2O_2$ least-squares plane are bent at the O1–O2 edge with a dihedral angle of 13.6(1)°.

$[CuNi(L^{2;2})(CH_3CN)](PF_6)_2 \cdot CH_3CN$ (3′). An ORTEP view of **3′** is shown in Fig. 6 together with the atom numbering scheme. The relevant bond distances and angles are given in Table 6.

The complex has a discrete heterodinuclear core with the Cu in the aminic site and Ni in the iminic site; the Cu–Ni interme-

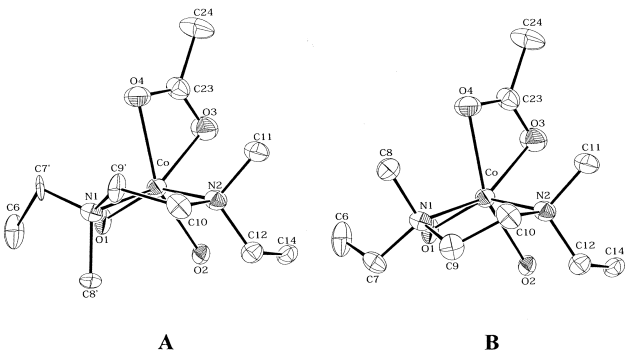

Fig. 4. Two distinct configurations of **1**. The probability of **A** is 75% and that of **B** is 25%.

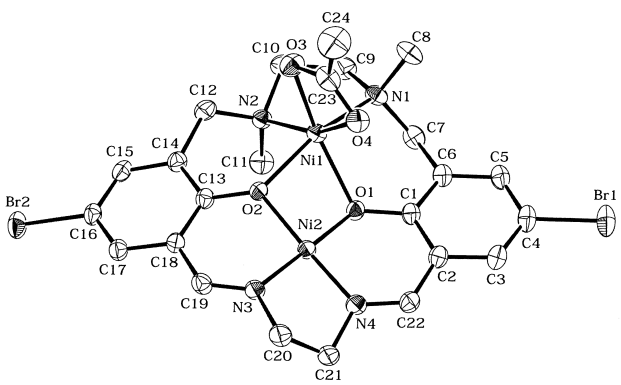

Fig. 5. An ORTEP view of $[NiNi(L^{2;2})(AcO)]PF_6$ (**2**) with the atom numbering scheme.

Table 5. Selected Bond Lengths (Å) and Angles (°) for $[NiNi(L^{2;2})(AcO)]PF_6$ (**2**)

Ni(1)–O(1)	2.098(4)	Ni(2)–O(1)	1.861(4)
Ni(1)–O(2)	2.094(4)	Ni(2)–O(2)	1.848(3)
Ni(1)–O(3)	2.076(4)	Ni(2)–N(3)	1.837(4)
Ni(1)–O(4)	2.117(4)	Ni(2)–N(4)	1.820(4)
Ni(1)–N(1)	2.102(4)		
Ni(1)–N(2)	2.058(4)	Ni(1)···Ni(2)	2.982(1)
Ni(1)–O(1)–Ni(2)	97.6(2)	O(3)–Ni(1)–N(1)	99.8(2)
Ni(1)–O(2)–Ni(2)	98.1(2)	O(3)–Ni(1)–N(2)	95.5(2)
O(1)–Ni(1)–O(2)	73.9(1)	O(4)–Ni(1)–N(1)	98.2(2)
O(1)–Ni(1)–O(3)	151.0(2)	O(4)–Ni(1)–N(2)	158.6(2)
O(1)–Ni(1)–O(4)	89.3(2)	N(1)–Ni(1)–N(2)	85.4(2)
O(1)–Ni(1)–N(1)	92.3(2)		
O(1)–Ni(1)–N(2)	111.8(2)	O(1)–Ni(2)–O(2)	85.6(1)
O(2)–Ni(1)–O(3)	99.4(2)	O(1)–Ni(2)–N(3)	174.5(2)
O(2)–Ni(1)–O(4)	96.6(1)	O(1)–Ni(2)–N(4)	94.9(2)
O(2)–Ni(1)–N(1)	159.6(2)	O(2)–Ni(2)–N(3)	92.8(2)
O(2)–Ni(1)–N(2)	86.0(1)	O(2)–Ni(2)–N(4)	175.4(2)
O(3)–Ni(1)–O(4)	63.1(2)	N(3)–Ni(2)–N(4)	87.1(2)

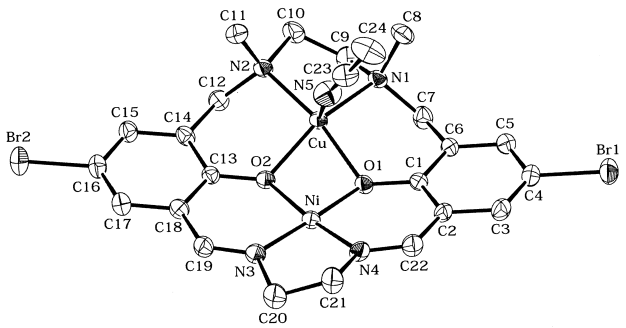

Fig. 6. An ORTEP view of $[CuNi(L^{2;2})(CH_3CN)](PF_6)_2 \cdot CH_3CN$ (**3′**) with the atom numbering scheme.

Table 6. Selected Bond Lengths (Å) and Angles (°) for $[CuNi(L^{2;2})(CH_3CN)](PF_6)_2 \cdot CH_3CN$ (**3′**)

Cu–O(1)	1.960(3)	Ni–O(1)	1.850(3)
Cu–O(2)	1.962(3)	Ni–O(2)	1.847(3)
Cu–N(1)	1.977(4)	Ni–N(3)	1.819(4)
Cu–N(2)	1.982(4)	Ni–N(4)	1.828(4)
Cu–N(5)	2.267(5)	Cu···Ni	2.820(3)
Cu–O(1)–Ni	95.4(1)	N(1)–Cu–N(2)	90.0(2)
Cu–O(2)–Ni	95.5(1)	N(1)–Cu–N(5)	102.9(2)
O(1)–Cu–O(2)	75.1(1)	N(2)–Cu–N(5)	102.5(2)
O(1)–Cu–N(1)	95.3(1)	O(1)–Ni–O(2)	80.6(1)
O(1)–Cu–N(2)	165.8(1)	O(1)–Ni–N(3)	176.0(2)
O(1)–Cu–N(5)	89.2(2)	O(1)–Ni–N(4)	95.9(2)
O(2)–Cu–N(1)	157.3(1)	O(2)–Ni–N(3)	95.7(2)
O(2)–Cu–N(2)	95.1(1)	O(2)–Ni–N(4)	173.0(2)
O(2)–Cu–N(5)	97.6(2)	N(3)–Ni–N(4)	88.0(2)

tallic separation is 2.820(3) Å. One acetonitrile molecule is bonded to the Cu providing a five-coordinate geometry about the metal ion. The equatorial Cu–O and Cu–N bond distances range from 1.960(3) to 1.982(4) Å. The axial Cu–N(5) bond distance is elongated (2.267(5) Å). The Cu is 0.289(2) Å displaced from the basal $N(amine)_2O_2$ least-squares plane toward N5. The geometry about the Ni is essentially planar with the Ni-to-donor bond distances ranging from 1.820(4) to 1.849(3) Å. The $N(amine)_2O_2$ least-squares plane and the $N(imine)_2O_2$ least-squares plane are bent at the O1–O2 edge with a dihedral angle of 27.3(1)°. The asymmetric nitrogen atoms N1 and N2 have *S* and *R* configuration, respectively. The two methyl groups attached to N1 and N2 are situated *cis* with respect to the mean molecular plane.

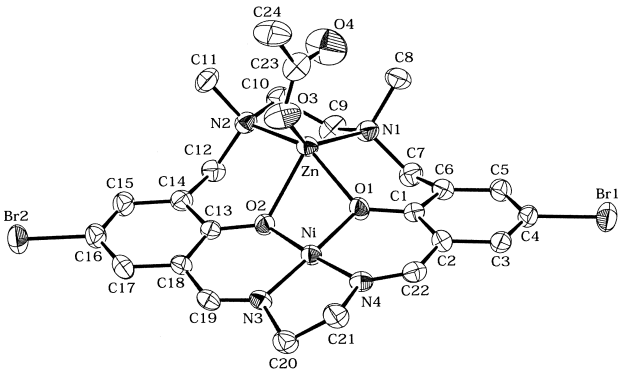

Fig. 7. An ORTEP view of $[ZnNi(L^{2;2})(AcO)]PF_6 \cdot CH_3CN$ (**4**) with the atom numbering scheme.

Table 7. Selected Bond Lengths (Å) and Angles (°) for $[ZnNi(L^{2;2})(AcO)]PF_6 \cdot CH_3CN$ (**4**)

Zn–O(1)	2.085(4)	Ni–O(2)	1.851(4)
Zn–O(2)	2.182(4)	Ni–N(3)	1.817(5)
Zn–O(3)	1.950(6)	Ni–N(4)	1.826(5)
Zn–N(1)	2.110(5)		
Zn–N(2)	2.130(5)	Zn···O(4)	2.647(11)
Ni–O(1)	1.810(4)	Zn···Ni	3.039(1)
Zn–O(1)–Ni	102.3(2)	O(3)–Zn–N(1)	139.4(3)
Zn–O(2)–Ni	97.5(2)	O(3)–Zn–N(2)	104.6(2)
O(1)–Zn–O(2)	67.4(2)	N(1)–Zn–N(2)	88.2(2)
O(1)–Zn–O(3)	100.6(2)	O(1)–Ni–O(2)	80.7(2)
O(1)–Zn–N(1)	86.8(2)	O(1)–Ni–N(3)	177.2(2)
O(1)–Zn–N(2)	146.5(2)	O(1)–Ni–N(4)	95.4(2)
O(2)–Zn–O(3)	95.7(2)	O(2)–Ni–N(3)	96.6(2)
O(2)–Zn–N(1)	123.5(2)	O(2)–Ni–N(4)	176.0(2)
O(2)–Zn–N(2)	88.3(2)	N(3)–Ni–N(4)	87.4(2)

$[ZnNi(L^{2;2})(AcO)]PF_6 \cdot CH_3CN$ (4). An ORTEP view of **4** is given in Fig. 7 together with the atom numbering scheme. The relevant bond distances and angles are given in Table 7.

The complex has a discrete heterodinuclear core with the Zn in the aminic site and the Ni in the iminic site, in the Ni–Zn intermetallic separation of 3.039(1) Å. The Zn in the aminic site has a square-pyramidal geometry with a unidentate acetate group at the axial site. The Zn-to-donor bond distances range from 1.950(6) to 2.182(4) Å. The Zn is 0.796(3) Å displaced from the basal $N(amine)_2O_2$ least-squares plane toward the acetate oxygen. The Ni in the iminic site has a planar geometry with the Ni-to-donor bond distances of 1.810(4)–1.851(4) Å. The $N(amine)_2O_2$ and $N(imine)_2O_2$ least-squares planes are bent at the O1–O2 edge with a dihedral angle of 12.5(2)°. The

asymmetric nitrogen atoms N1 and N2 have *S* and *R* configuration, respectively. The two methyl groups attached to N1 and N2 are situated *cis* with respect to the $N(amine)_2O_2$ plane.

Comment about Metal Substitution Reaction. The above X-ray crystallographic results clearly indicate that the metal substitution reaction of $[PbNi(L^{2;2})(AcO)_2]$ with M^{II} sulfate affords the $M^{II}Ni^{II}$ complexes (**1**–**4**). This differs from the metal substitution reaction of $[PbCu(L^{m;n})](ClO_4)_2$ with M^{II} sulfate, where the Cu migrates from the iminic site to the aminic site affording $Cu^{II}M^{II}$ complexes.[2b] It is supposed that $[PbCu(L^{m;n})](ClO_4)_2$ binds M^{II} ion through the two phenolic oxygen atoms to form a di(μ^3-phenoxo) $Pb^{II}Cu^{II}M^{II}$ complex and thence the M^{II} moves to the iminic site with concomitant migration of the Cu to the aminic site and release of the Pb from the aminic site.[2d,2e] In the present case the metal substitution reaction may proceed by a dissociative mechanism, because the *cis* arrangement of the two *N*-methyl groups in the PbNi precursor complex changes to the *trans* arrangement in **1** (form B) and **2**. The X-ray crystallography for $[PbNi(L^{2;2})(AcO)_2]$ indicates that the Ni is bound to the iminic site in short bond distances (1.817(8)–1.842(9) Å), whereas the Pb is loosely bound to the aminic site as inferred from the long Pb–N1 and Pb–O1 bond distances (2.967(8) and 3.047(7) Å, respectively). Such structural features of the PbNi complex can explain the facile substitution of the Pb^{II} in the aminic site for M^{II} while maintaining the Ni in the iminic site.

Physicochemical Properties. The room-temperature magnetic moments of **1**, **2** and **3** are 4.98, 3.17 and 1.87 μ_B, respectively, which are common for isolated Co^{II} ($S = 3/2$), Ni^{II} ($S = 1$) and Cu^{II} ($S = 1/2$), respectively. Complex **4** is diamagnetic. Evidently the Ni^{II} in the iminic site is diamagnetic in all the complexes.

Visible absorption spectra of **1**–**4** in DMF are characterized by an absorption band at ~520 nm that is typical of planar Ni^{II} in the iminic site.[8] Complex **1** (CoNi) shows a discernible shoulder near 1240 nm that is attributed to a d–d component of the Co^{II} ion. Complex **2** (NiNi) shows two additional bands at 652 and 1030 nm attributable to the d–d components of the Ni^{II} ion in the aminic site. Complex **3** (CuNi) has a distinct absorption band at 670 nm due to the Cu^{II} in the aminic site.

Electrochemical properties of **1**–**4** were studied in acetonitrile by means of cyclic voltammetry. Complexes **1**, **2** and **4** each show a reversible or quasi reversible couple at 1.29 ± 0.05 V (vs Ag/Ag^+) attributable to the Ni^I/Ni^{II} redox process in the iminic site.[11] Complex **3** shows two redox couples at −0.08 and −1.57 V. The former can be attributed to the Cu^I/Cu^{II} redox process at the aminic site.[2] The high potential of the Cu^I/Cu^{II} process can be ascribed to the distorted $\{CuN_2O_2\}$ environment favorable for Cu^I.[12] The second couple at −1.57 V of **3** is assigned to the Ni^I/Ni^{II} process that occurs at low potential relative to those for **1**, **2,** and **4**. This is because the reduction of the Ni in **3** accompanies a charge change of $\{Ni^{II}Cu^I\}^-/\{Ni^ICu^I\}^{2-}$ and this change is energetically more difficult than the charge change of $\{Ni^{II}M^{II}\}^0/\{Ni^IM^{II}\}^-$ accompanied by the Ni reduction of **1**, **2** and **4**.

Anomalous EPR of 3′ by Coordination of 1-Methylimidazole. We have noticed that a reddish DMF solution of **3** and **3′** assumes a green color when 1-methylimidazole (MeIm) is added to each solution. Detailed studies on the color change with MeIm have been carried out for **3′** of known structure.

The EPR spectrum of **3′** in a frozen DMF solution at liquid nitrogen temperature (Fig. 8, trace **a**), with $g_\parallel = 2.29$, $g_\perp = 2.06$ and $A_\parallel = 150 \times 10^{-4}$ cm^{-1}, is typical of isolated Cu^{II} under an axially distorted geometry.[13] If one equivalent of MeIm was added to the solution, the original EPR signals were mostly replaced by new EPR signals of $g_\parallel = 2.06$ and $g_\perp = 2.26$ with a multi-line structure ($A_\parallel = 15.8 \times 10^{-4}$ cm^{-1}) superimposed on the $g_\parallel$ component (trace **b**). The multi-line structure suggests that MeIm is involved in the interaction with unpaired electrons. In our EPR simulation, the multi-line structure could be well reproduced with $A_\parallel(Cu) = 50 \times 10^{-4}$ cm^{-1} and $A_\parallel(N) = 15.0 \times 10^{-4}$ cm^{-1} (see the insert of Fig. 8). The A_{Cu} value is one third of that of trace **a**. This fact and the EPR pattern of $g_\perp > g_\parallel$ suggest that the EPR signal is associated with the spin-doublet ground state ($S_T = 1/2$) of antiferromagnetically coupled $Cu^{II}(S = 1/2)$–$Ni^{II}(S = 1)$.[2b,14–16] It is most likely that MeIm coordinates to an axial site of the Ni^{II} to cause the spin conversion from $S = 0$ to $S = 1$ and the antiferromagnetic interaction between the Cu^{II} and $Ni^{II}(S = 1)$ is strong enough so as to allow thermal population only on the spin-doublet ground state at liquid nitrogen temperature.

The spin conversion of Ni^{II} ($S = 0$) into Ni^{II} ($S = 1$) by MeIm coordination is supported from visible spectral studies

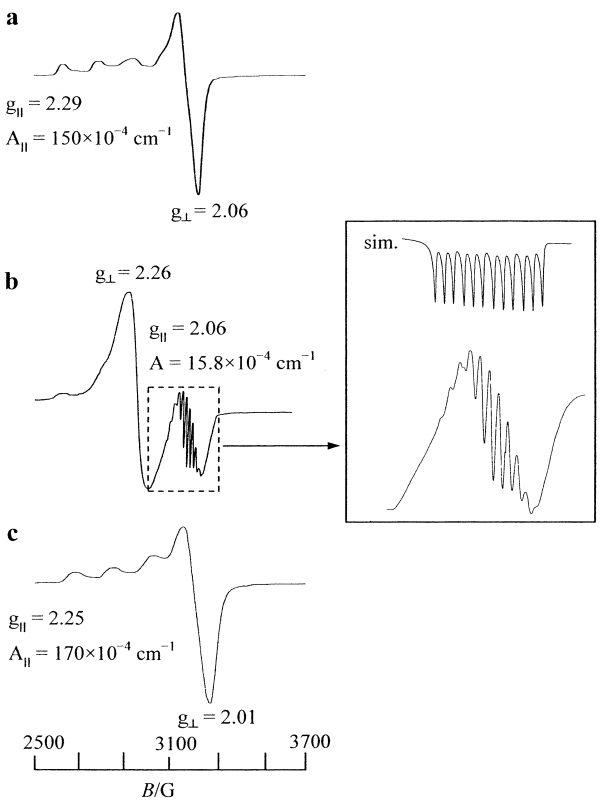

Fig. 8. EPR spectra of **3′** in frozen DMF solution at liquid nitrogen temperature; (**a**) in the absence of MeIm, (**b**) in the presence of one equivalent of MeIm, and (**c**) in the presence of two equivalents of MeIm. The insert is an expansion of the $g_\parallel$ component of **b** (bottom) and a simulated EPR with $A_\parallel(Cu) = 50.0\times10^{-4}$ cm^{-1} and $A_\parallel(N) = 15.0\times10^{-4}$ cm^{-1} (top).

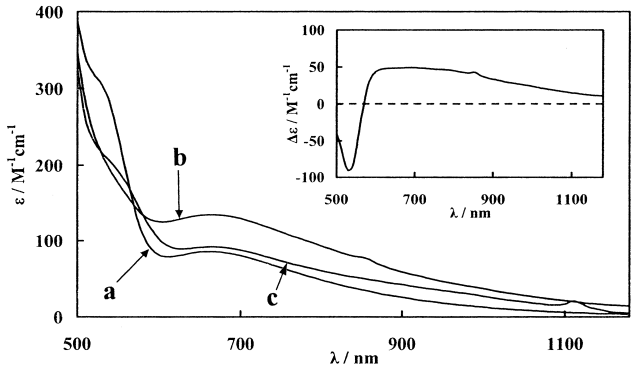

Fig. 9. Visible spectra of **3′** in DMF; (**a**) in the absence of MeIm, (**b**) in the presence of one epuivalent of MeIm and (**c**) in the presence of two epuivalents of MeIm. The insert is the difference spectrum between **a** and **b**.

(Fig. 9). The trace **a** of Fig. 9 is the visible spectrum of **3′** in DMF, showing the d–d band of the low-spin Ni^{II} ion at 520 and the d–d band of the Cu^{II} ion at 670 nm. On adding one equivalent of MeIm to the solution (trace **b**), the absorption band due to the low-spin Ni^{II} disappears (see difference spectrum in the insert). The enhancement in the region of 600–1000 nm may result from some geometrical change about the Cu^{II} and the occurrence of d–d transition bands of the high-spin Ni^{II} in this region. The preferential coordination of MeIm to the Ni^{II} centre is not strange when the spin conversion Ni^{II} ($S = 0$) → Ni^{II} ($S = 1$) is taken into consideration. That is, high-spin Ni^{II} strongly binds a fifth donor, whereas Cu^{II} weakly binds a fifth donor due to the Jahn–Teller effect of d^9 electronic configuration.

When two equivalents of MeIm were added, the solution assumed an orange color and showed an axial pattern of EPR typical of magnetically isolated Cu^{II} (trace **c**). This means that the Ni^{II} is diamagnetic in this solution. The electronic spectrum exhibiting a discernible shoulder at ~530 nm (Fig. 9, **c**) is also consistent with the low-spin state of the Ni^{II}. When the solution was diffused with 2-propanol, orange microcrystals of [Ni($L^{2;2}$)] precipitated; they were identified by IR spectra in comparison with the authentic sample. Thus, the Cu^{II} is eliminated from the aminic site on adding two equivalents of MeIm.

It is important to consider why such coordination of MeIm to the axial site of the M^{II} does not occur in other complexes (**1**, **2** and **4**). In the comparison of the crystal structures of **1**, **2**, **3′** and **4**, no prominent geometrical difference is observed in the {Ni(imine)$_2$O$_2$} chromophore. For example, the average of the Ni–N and Ni–O bond distances is 1.832 Å for **1**, 1.842 Å for **2**, 1.836 Å for **3′** and 1.825 Å for **4**. One noticeable difference is in the M–O bond distance in the aminic site. That is, the average Cu–O bond distance of **3′** is 1.961 Å, which is very short relative to the average M–O bond distances of **1**, **2** and **4** (2.096–2.134 Å). It is most likely that in the case of **3′** (and **3**) the strong Cu–O bond reduces the electron density on the phenolic oxygen atoms and thence weakens the ligand field strength of the {NiN(imine)$_2$O$_2$} chromophore. Similar axial coordination of pyridine to planar Ni^{II} has been recognized for dinuclear $Ni^{II}M^{II}$ (M = Ni, Zn) complexes of analogous macrocyclic ligands (see Chart 2), where a short M-to-donor bond is established by X-ray crystallography.[17]

In conclusion, the CuNi complex **3′** (and **3** also) combines

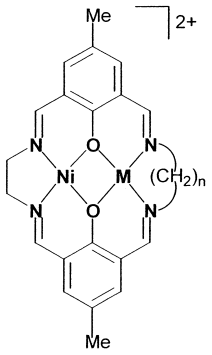

Chart 2. Chemical structure of $Ni^{II}M^{II}$ complexes with $(R^{m;n})^{2-}$.

MeIm at the axial site of the Ni^{II} to cause the spin conversion of Ni^{II} ($S = 0$) into Ni^{II} ($S = 1$). A strong antiferromagnetic interaction operates between Cu^{II} ($S = 1/2$) and Ni^{II} ($S = 1$) in the resulting MeIm adduct, affording the spin-doublet ground state ($S_T = 1/2$). The EPR spectrum for the spin-doublet ground state indicates that one unpaired electron exists on the molecular orbital comprised of d_{Z^2}(Cu) and d_{Z^2}(Ni) and is delocalized over the two metal ions.

This work was supported by a Grant-in-Aid for Scientific Research on Priority Area "Metal-assembled Complexes" (No. 10149106) and a Grant-in-Aid for COE Research "Design and Control of Advanced Molecular Assembly System" (No. 08CE2005) from the Ministry of Education, Science, Sports and Culture.

References

1 H. Ōkawa, H. Furutachi, and D. E. Fenton, *Coord. Chem. Rev.*, **174**, 51 (1998).

2 a) M. Yonemura, Y. Matsumura, M. Ohba, H. Ōkawa, and D. E. Fenton, *Chem. Lett.*, **1996**, 601. b) M. Yonemura, Y. Matsumura, H. Furutachi, M. Ohba, H. Ōkawa, and D. E. Fenton, *Inorg. Chem.*, **36**, 2711 (1997). c) M. Yonemura, M. Ohba, K. Takahashi, H. Ōkawa, and D. E. Fenton, *Inorg. Chim. Acta.*, **283**, 72 (1998). d) M. Yonemura, Y. Nakamura, N. Usuki, and H. Ōkawa, *Proc. Ind. Acad. Sci.*, **112**, 291 (2000). e) M. Yonemura, N. Usuki, Y. Nakamura, M. Ohba, and H. Ōkawa, *J. Chem. Soc., Dalton Trans.*, **2000**, 3624.

3 C. Fraser, L. Johnston, A. L. Rheingold, B. S. Haggerty, G. K. Williams, J. Whelan, and B. Bosnich, *Inorg. Chem.*, **31**, 1835 (1992); D. G. McCollum, G. P. A. Yap, A. L. Rheingold, and B. Bosnich, *J. Am. Chem. Soc.*, **118**, 1365 (1996), and references therein.

4 S. Karunakaran and M. Kandaswamy, *J. Chem. Soc., Dalton Trans.*, **1994**, 1595.

5 E. V. Rybak-akimova, N. W. Alcock, and D. H. Busch, *Inorg. Chem.*, **37**, 1563 (1998).

6 E. A. Boudreaux and L. N. Mulay, "Theory and Applications of Molecular Paramagnetism," Wiley (1976), p.491.

7 TEXSAN, Molecular Structure Analysis Package, Molecular Structure Corporation, Houston, TX, 1985 and 1992.

8 a) S. M. Crawford, Spectrochim. Acta, **19**, 255 (1963). b) R. H. Holm, *J. Am. Chem. Soc.*, **82**, 5632 (1960). c) B. Bosnich, *J. Am. Chem. Soc.*, **90**, 627 (1968). d) R. S. Downing and F. L.

Urbach, *J. Am. Chem. Soc.*, **92**, 5861 (1970).
9 C. K. Johnson, Report 3794, Oak Ridge National Laboratory, Oak Ridge, TN, 1965.
10 L. M. Shkol'nikova, E. M. Yumal', E. A. Shugan, and V. A. Voblikova, *J. Struct. Chem. (USSR)*, **11**, 819 (1970).
11 a) G. Gosden, K. P. Healy, and D. Pletcher, *J. Chem. Soc., Dalton Trans.*, **1978**, 972. b) B. M. Higson and E. D. McKenzie, *Inorg. Nucl. Chem. Lett.*, **6**, 209 (1970).
12 G. S. Patterson and R. H. Holm, *Bioinorg. Chem.*, **4**, 257 (1975).
13 B. A. Goodman and J. B. Raymor, *Adv. Inorg. Chem. Radiochem.*, **13**, 135 (1970).
14 R. P. Scaringe, D. J. Hodgson, and W. E. Hatfield, *Mol. Phys.*, **35**, 701 (1978).
15 E. Buluggiu, *J. Phys. Chem. Solids*, **41**, 1175 (1980).
16 T. Aono, H. Wada, Y. Aratake, N. Matsumoto, H. Ōkawa, and Y. Matsuda, *J. Chem. Soc., Dalton Trans.*, **1996**, 25.
17 H. Ōkawa, Y. Aratake, K. Motoda, M. Ohba, H. Sakiyama, and N. Matsumoto, *Supramol. Chem.*, **6**, 293 (1996).